Structural Behavior of All-FRP Beam-Column Plate-Bolted Joints

Francesca Feroldi, Ph.D.[1]; and Salvatore Russo[2]

Abstract: Fiber-reinforced polymer (FRP) material is very interesting for its use as the sole material in the construction of structures because of its remarkable lightness, which reduces seismic forces; its ease of assembly; and its durability. All-FRP structures use bolted connections to form nodes between columns and beams, particularly steel bolts. This research focuses on the use of FRP pultruded plates instead of web and flange cleats for bolted beam-to-column joints. Currently, angles and bolts between columns and beams are widely employed, whereas bolted plates are still a novelty. Both experimental and numerical studies of two different configurations of bolted connections made by pultruded plates and C-shape FRP profiles demonstrated that the plates have considerable influence on the moment-rotation response of joints so that the joint's failure mode involves mainly the bolted plate. The experimental program in this paper determined the initial stiffness of each connection, the ultimate moment capacity, and the rotation associated with the ultimate strength. These results were then compared against numerical predictions obtained using a commercial code for finite-element analysis. **DOI: 10.1061/(ASCE)CC.1943-5614.0000667.**

Author keywords: All-glass fiber–reinforced polymer (GFRP) bolted joints; Beam-to-column bolted joints; Pultruded bolted plate; Progressive failure analysis.

Introduction

In recent years, fiber-reinforced polymer (FRP) composites have emerged as an interesting construction material in the civil sector, mainly because of their high strength-to-weight and stiffness-to-weight ratios, corrosion resistance, high durability, and high adaptability to different contexts and design needs (Agarwal et al. 2006; ASCE 1984). They are interesting for the renewal of existing structures, especially in the rehabilitation of concrete structures such as buildings or bridges, and for new construction. Recent seismic events have emphasized the importance of seismic retrofits for existing structures throughout the world. As a matter of fact, one of the main current uses of this material is in strengthening concrete structures by means of externally bonded FRP reinforcement.

In addition to the consolidated use of FRP composites, a growing new technology is the design of all-FRP construction by means of structural pultruded profiles. Because of its mechanical properties, glass fiber–reinforced polymer (GFRP) is an alternative to conventional construction materials such as steel or wood (Bank 2006; Boscato et al. 2011). The most widely known applications of GFRP are foot and road bridges (Keller 2003; Adilardi and Russo 2010; Boscato and Russo 2008), temporary and emergency framed structures (Dicuonzo et al. 2008), and independent lightweight structures in existing buildings (Keller 2003; Boscato and Russo 2009, 2013). It can also be used to increase the bending stiffness of existing floors with a very modest increase in weight or to build superimposed structures without excessive overload. However, all-GFRP construction is limited by its structural joints, which represent structural discontinuities associated with stress localization.

Structural joints can be bonded or bolted; nevertheless, they often represent a gap in structural behavior because of their failure mode. Typically, bolted beam-to-column joints are formed using web cleats, web and flange cleats, GRP bolts, and, more frequently, steel bolts. The behavior of bolted connections between composite profiles is influenced by factors such as high-stress concentrations near bolt holes, no yielding capability, and reduced strength due to cleavage, net tension, shear-out, and bearing-mode failures (Turvey and Wang 2008). Because the capacity of a structure is often limited by the capacity of its connections, an understanding of connection behavior is crucial and needs to be fully investigated.

In the last two decades, many studies have characterized connections between pultruded FRP elements. Reviews of experimental tests on bolted pultruded joints were conducted by Mottram and Zheng (1996) and Turvey and Cooper (2004). They showed that the behavior of bolted connections is substantially described by the moment-rotation plot (M-θ). The M-θ response in beam-to-column joints is generally dominated by the moment M caused by loading on the beam and the rotation θ that is equal to the difference between the beam's end rotation and the column's rotation.

Experimental tests show that initial joint stiffness is determined by the stiffness of the connecting components, which are often GRP angle cleats rather than bolts. When steel bolts are used in these joints, they are generally sufficiently large to prevent failure of the bolt shank in shear; thus, they remain elastic. As rotation increases, the M-θ response becomes nonlinear because of progressive damage to pultruded components. The ultimate failure of bolted GRP joints is usually associated with brittle material failure, the form of which depends on both the relative strength of each element and the configuration of the joint. Recent work on FRP bolted connections (e.g., Qureshi and Mottram 2013, 2014, 2015) focused on the behavior of a beam-to-column joint connected to a central column through a pair of web cleats. Test results demonstrated that joints with FRP cleats failed because of

[1]Dept. of Construction, IUAV Univ. of Venice, Dorsoduro 2206, 30123 Venice, Italy (corresponding author). E-mail: feroldifrancesca@gmail.com

[2]Associate Professor of Structural Civil Engineering, Dept. of Construction, IUAV Univ. of Venice, Dorsoduro 2206, 30123 Venice, Italy. E-mail: russo@iuav.it

Note. This manuscript was submitted on July 16, 2015; approved on October 30, 2015; published online on January 8, 2016. Discussion period open until June 8, 2016; separate discussions must be submitted for individual papers. This paper is part of the ***Journal of Composites for Construction***, © ASCE, ISSN 1090-0268.

Fig. 1. Details of a PFRP-steel connection in the spatial structure covering the S. Maria Paganica church after the earthquake

delamination cracking at the top of the cleats; when the cleats were of steel, FRP failure occurred inside the column members. Based on these results, the most critical points in a beam-to-column bolted connection were demonstrated to be those near the fillet radius of a FRP web cleat, where tension, delamination cracking, and tensile tearing can occur.

This paper focuses on experimental and numerical studies of innovative beam-to-column joints connecting two C-shape PFRP profiles by means of a gusset bolted plate placed between the webs of the elements. This configuration is significantly different from traditional configurations because stresses and deformations are transferred from the column to the beam not through a web cleat but through a gusset plate. Reference is made to joints used for a covering structure of a historic church, S. Maria Paganica, that stroked and partially collapsed after the L'Aquila (Italy) earthquake on April 4, 2009 (Boscato et al. 2012; Russo 2013). The all-FRP spatial-reticular structure of the church comprised elements realized through a composite cross section made by four C-shape bolted PFRP profiles; the assembly of structural profiles was made using FRP plates and steel bolts. The joint design was totally different from traditional design because the assembly of steel and FRP drew on a new hierarchy of strength and collapse mechanisms (Russo 2011, 2012). Fig. 1 shows the PFRP structure inside the church.

On the basis of the joints used in S. Maria Paganica, simplified beam-to-column connections were tested in the laboratory with in-plane loading to evaluate the moment-rotation response of joints composed of very light and elastic-brittle material. This evaluation was very innovative because recommendations for an analytical approach to PFRP structures in seismic zones are still in progress. The first configuration comprised two C-shape PFRP profiles of size $152 \times 43 \times 9.5$ mm, similar to those used in the nave of the church; the second configuration was realized by means of two "C-shape PFRP profiles of size $200 \times 60 \times 10$ mm, similar to those placed in the apse. Because the second-order instability in compressed members had to be avoided (Di Tommaso and Russo 2003), the column where the load was applied was stiffened by means of bolted plates against out-of-plane deformations.

The stress test configuration did not provide the same stress state of the spatial-reticular elements because the bolted connections were studied only under in-plane loading; therefore, the configuration could provide the moment-rotation response of the node without the effect of lateral torsional buckling failure or out-of-plane instability.

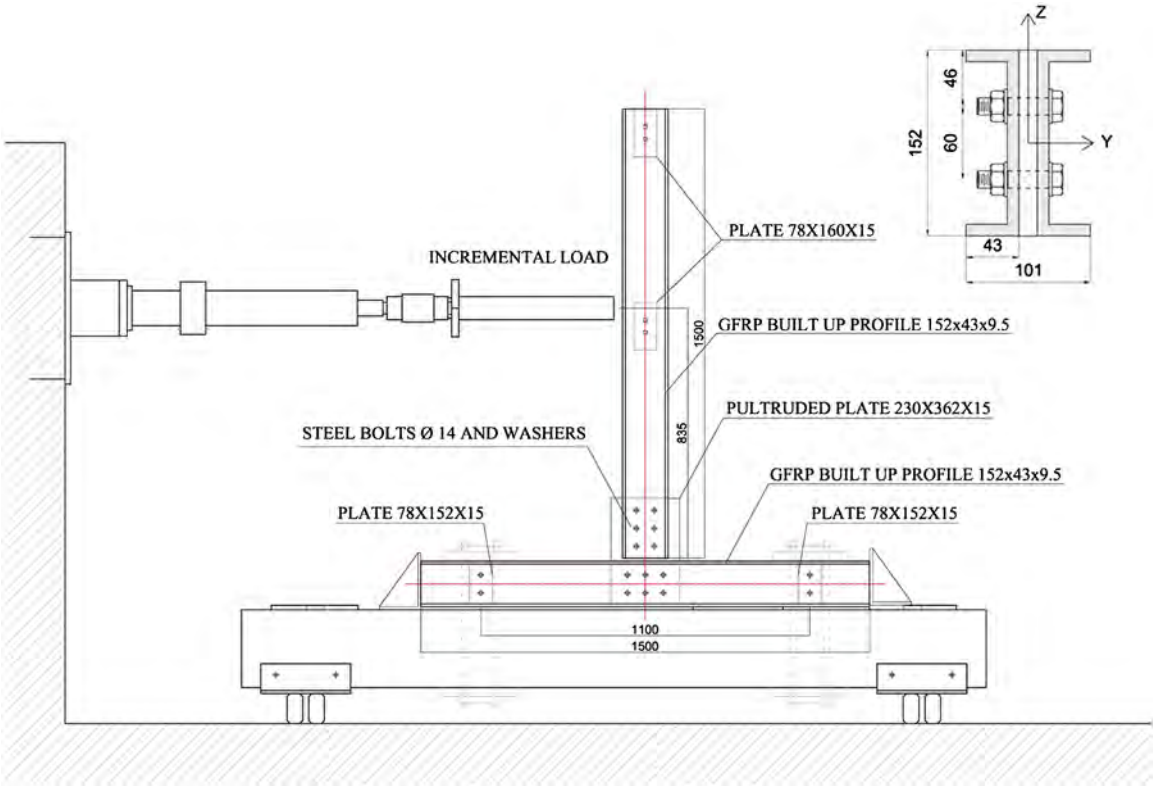

Fig. 2. Connection A: geometry and test setup (mm)

Experimental Program

Specimens and Experimental Setup

The main purpose of this experimental study was to analyze the effects of a monotonic unidirectional load on the behavior of two types of beam-to-column joints. In the first configuration, the A connection, both the beam and the column comprised two "C"-shape PFRP profiles of size $152 \times 43 \times 9.5$ mm and length 1,500 mm; the profiles were joined by four bolted plates of size $78 \times 152 \times 15$ mm placed between them. The joint was realized by means of a gusset plate of size $230 \times 362 \times 15$ mm that connected the bottom of the column with the center of the beam through 12 partially threaded Φ14-mm steel bolts and washers (Fig. 2). The beam was simply supported at two points separated by a distance of 1,100 mm.

The instrumentation used for testing and evaluating the behavior of the joints consisted of 10 strain gauges, 4 displacement transducers, and 2 inclinometers, placed as shown in Fig. 3: the inclinometers located on the web of the profiles (CH11 and CH12) allowed for reading rotations of each profile; the displacement transducers (CH13 and CH14) were employed to measure horizontal displacement in the direction of increasing force; and the remaining two displacement transducers (CH15 and CH16) were symmetrically placed on the beam flanges near the bolted plate to measure vertical displacements. The strain gauges placed around the bolts and on the plate were oriented according to the vertical and horizontal axes to check the state of plane stress as the load increased. In the experimental tests, under displacement control, the horizontal load was applied through a steel plate to a height of 835 mm from the bottom of the column.

The second connection (B) differed from the first one both in the geometry of the profiles and the bolted plate and in the number of steel bolts, but the test setup was the same. The beam and column comprised two C-shape PFRP profiles of size $200 \times 60 \times 10$ mm and length 1,500 mm joined by 4 bolted plates of size $76 \times 200 \times 15$ mm placed between them. The incremental load was applied at a distance of 811 mm from the bottom of the column. The geometrical characteristics are shown in Fig. 4. The joint was realized by means of a gusset plate of size $350 \times 433 \times 15$ mm that connected the beam and the column by 12 and 6 partially threaded Φ14-mm steel bolts, respectively. On Joint B, the instrumentation for monitoring local deformations was similar to that described for Node A (Fig. 5).

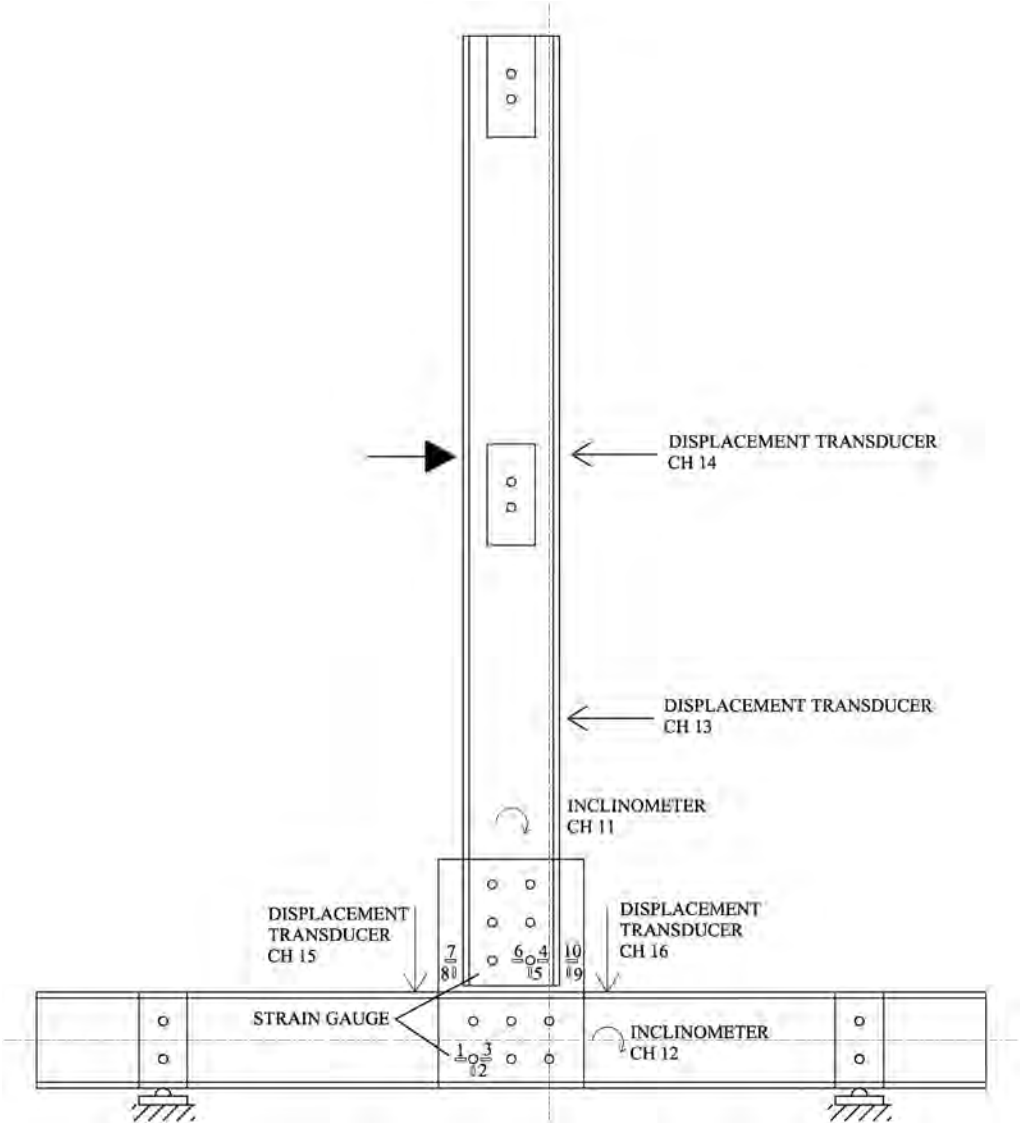

Fig. 3. Connection A: location of instrumentation

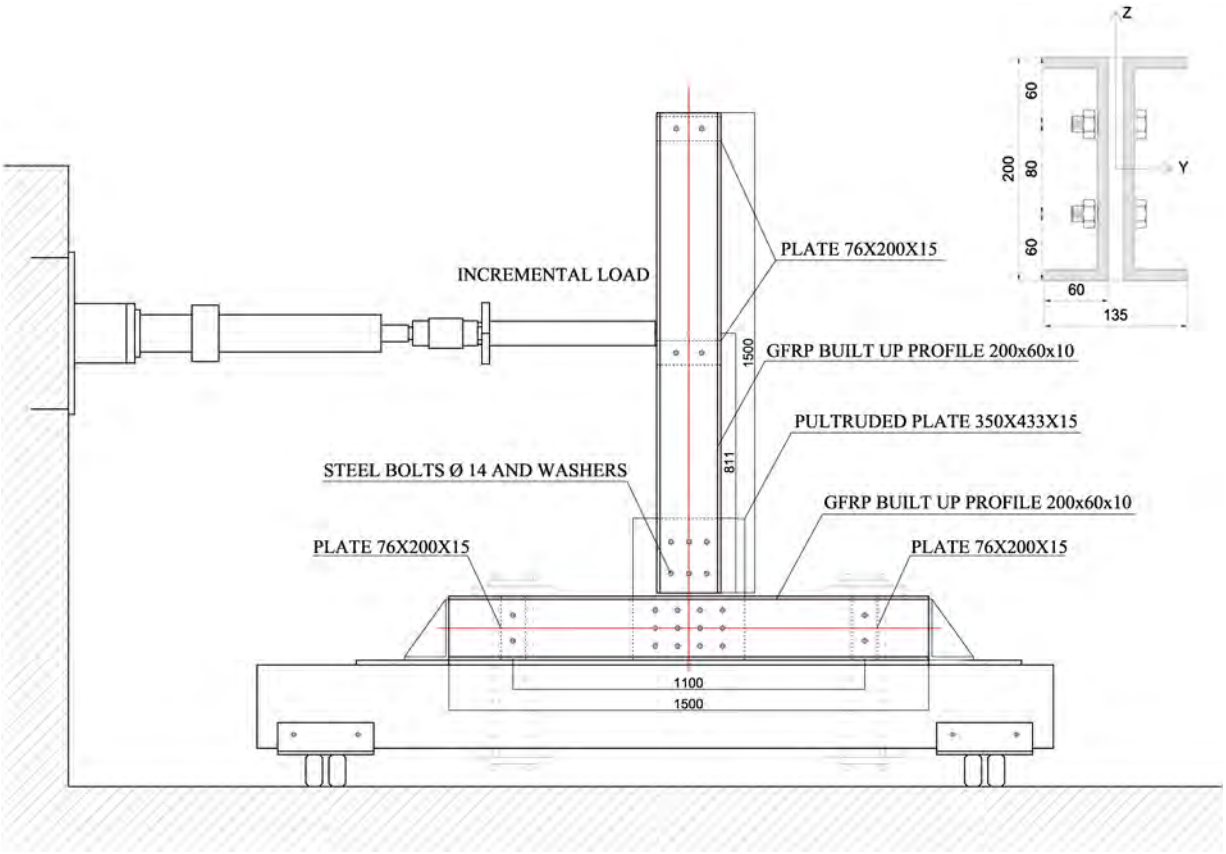

Fig. 4. Connection B: geometry and test setup (mm)

Before applying the horizontal load, torque had to be applied to the bolts to avoid the initial damage on the contact zone between the bolt shank and the section of the element due to crushing of the material in the direction perpendicular to the fibers (the direction in which the strength was lower). An initial tightening torque of 20 N · m was applied to all bolts, which corresponded to a prestress of 16 MPa on the surface contact between the washer and the profile. As for the initial tightening torque, in absence of applicable specific standards, reference is made to values proposed in the literature (Cooper and Turvey 1995; Khashaba et al. 2006)

Mechanical properties of the GFRP plates and profiles are shown in Tables 1–3. As for structural profiles, the x-axis represented the position along the longitudinal axis of the element (i.e., the direction of pultrusion), and the y- and z-axes defined the orientation of the cross-sectional plane of the element. The x-axis of the plates represented the direction perpendicular to the plane of the element, and the y-axis indicated the direction of the longitudinal fibers, oriented with respect to the largest dimension. The main results are described in the following sections.

Experimental Results for Joint A

To verify the behavior of the node under very low stresses, preliminary static tests with maximum horizontal displacements (D_{max}) of 10 mm and 20 mm were performed on Joint A. The joint underwent a significant decrease in stiffness between each loading cycle (it decreased by 30% between the first and second cycles and by 5% between the second and failure cycles) until a value of 194 kN · m was reached in the static failure test. This decrease in stiffness was due to progressive damage of the bolted plate, in which the bolt shank induced a bearing failure mode. The moment-rotation response obtained by the failure static test was affected by a gradual loss of stiffness as the deformation proceeded: a maximum moment of 12 kN · m was reached at a rotation of 0.11 rad. The column was then rigidly rotated under constant load until failure.

It was interesting to observe that the damage affected only the bolted plate whereas the structural profiles remained intact (Fig. 6). Because the global behavior of the node was heavily influenced by the bolted plate, the horizontal beam was not involved in the connection rotation; as a matter of fact, the two transducers, CH15 and CH16, which monitored any vertical deflection of the beam and were symmetrically located with respect to the bolted plate, recorded maximum vertical displacements of approximately 2.2 mm and 1 mm, respectively (Fig. 7). Even the inclinometers placed on the web of both the beam and the column confirmed what was observed: during the test, they recorded a maximum beam rotation of approximately (1.75×10^{-3}) rad whereas the column reached a rotation of 0.18 rad.

The torque values on each bolt were measured by a torque wrench after the failure static test; they varied from a minimum of 21 N · m to a maximum of 60 N · m. The highest torque values were recorded near Holes 3–9 and 12 (Fig. 8), where the compressive stress perpendicular to the fibers was greater than 40 MPa. The compressive stress due to tightening the torque of the other bolts ranged 25–40 MPa, with the exception of bolts 1–4 and 6, where it was less than 25 MPa. The maximum stress was still less than the nominal strength of a pultruded FRP profile in the plane perpendicular to the pultrusion direction (80 MPa).

In accordance with the applied load pattern, close to strain gauge 1 and 2, the profile was under tensile stresses in the direction perpendicular to the longitudinal axis and under compression stresses along the direction of pultrusion. In contrast, Strain Gauge

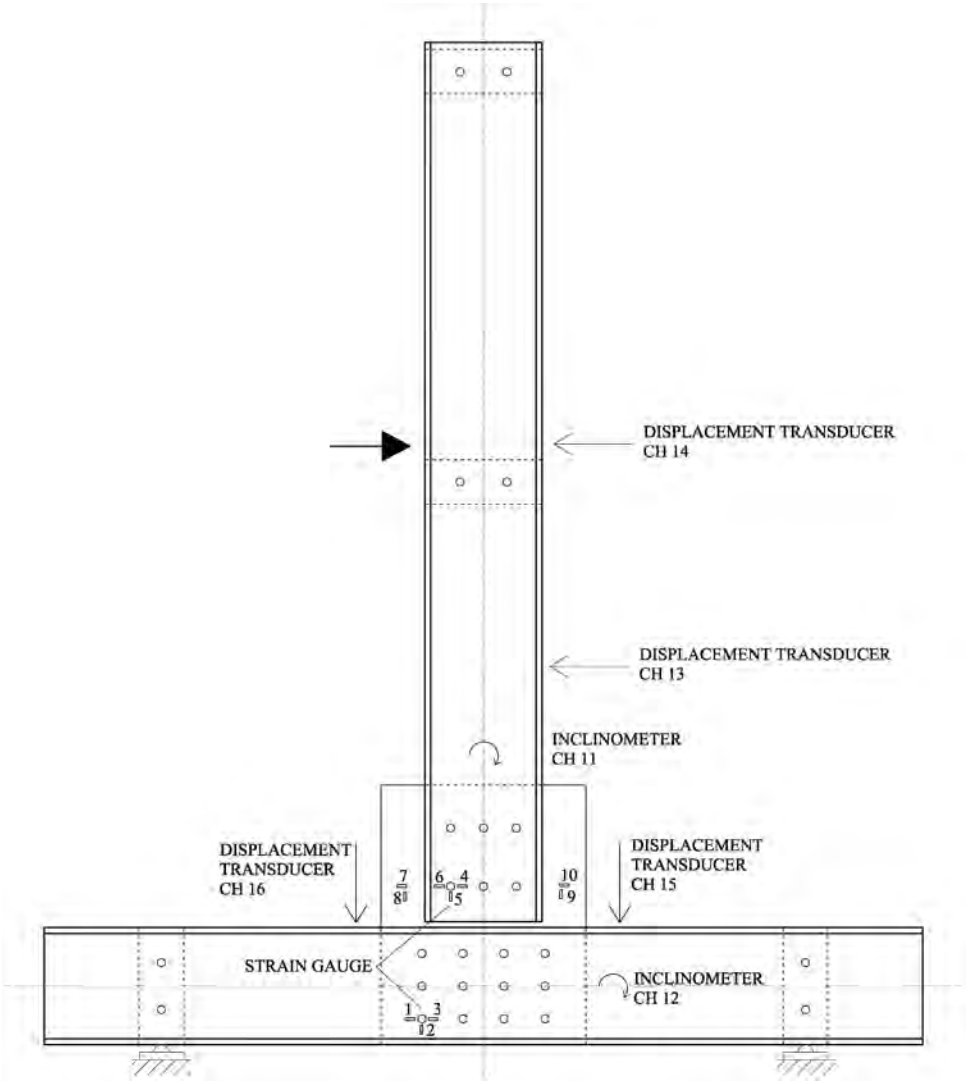

Fig. 5. Connection B: location of instrumentation

Table 1. Mechanical Properties of GFRP Pultruded Profiles of 200 × 60 × 10 mm

Property_FRP	Notation	Value
Longitudinal tensile modulus of elasticity	E_x	28.5 (GPa)
Transverse tensile modulus of elasticity	$E_y = E_z$	8.5 (GPa)
Transverse shear modulus of elasticity	G_{yz}	3.5 (GPa)
In-plane shear modulus of elasticity	$G_{xy} = G_{xz}$	2.5 (GPa)
Major Poisson's ratio	$\nu_{xy} = \nu_{xz}$	0.25
Minor Poisson's ratio	ν_{yz}	0.12
Bulk weight density of FRP	γ	1,850 (kg/m^3)
Longitudinal tensile strength	σ_{xt}	350 (MPa)
Transverse tensile strength	$\sigma_{yt} = \sigma_{zt}$	70 (MPa)
Longitudinal compressive strength	σ_{xc}	413 (MPa)
Transverse compressive strength	$\sigma_{yc} = \sigma_{zc}$	80 (MPa)
Shear strength	$\tau_{xy} = \tau_{xz} = \tau_{yz}$	40 (MPa)
	τ_{yz}	40 (MPa)

Table 2. Mechanical Properties of GFRP Pultruded Profiles of 152 × 43 × 9.5 mm

Property_FRP	Notation	Value
Longitudinal tensile modulus of elasticity	E_x	27 (GPa)
Transverse tensile modulus of elasticity	$E_y = E_z$	11 (GPa)
Transverse shear modulus of elasticity	G_{yz}	3.5 (GPa)
In-plane shear modulus of elasticity	$G_{xy} = G_{xz}$	2.5 (GPa)
Major Poisson's ratio	$\nu_{xy} = \nu_{xz}$	0.23
Minor Poisson's ratio	ν_{yz}	0.12
Bulk weight density of FRP	γ	1,850 (kg/m^3)
Longitudinal tensile strength	σ_{xt}	330 (MPa)
Transverse tensile strength	$\sigma_{yt} = \sigma_{zt}$	70 (MPa)
Longitudinal compressive strength	σ_{xc}	240 (MPa)
Transverse compressive strength	$\sigma_{yc} = \sigma_{zc}$	80 (MPa)
Shear strength	$\tau_{xy} = \tau_{xz}$	40 (MPa)
	τ_{yz}	40 (MPa)

4 was subject to tensile stresses and Strain Gauge 5 was subject to compressive stresses oriented with respect to the longitudinal axis of the column (Fig. 9). The monitored state of stress in the profiles was less than the ultimate strength of the material, confirming that both the beam and the column remained substantially intact during the test.

Experimental Results for Joint B

The failure static test on Joint B demonstrated that in preliminary tests with maximum displacements of 10 and 20 mm, the global stiffness remained constant. The ultimate resistance moment of the joint was 21 kN · m, and its flexural stiffness was approximately

Table 3. Mechanical Properties of GFRP Pultruded Plates

Property_PLATE	Notation	Value
Longitudinal tensile modulus of elasticity	E_y	27 (GPa)
Transverse tensile modulus of elasticity	$E_z = E_x$	10.5 (GPa)
Transverse shear modulus of elasticity	G_{xz}	3.5 (GPa)
In-plane shear modulus of elasticity	$G_{xy} = G_{yz}$	2.5 (GPa)
Major Poisson's ratio	$\nu_{xy} = \nu_{yz}$	0.25
Minor Poisson's ratio	ν_{xz}	0.12
Bulk weight density of FRP	γ	1,850 (kg/m^3)
Longitudinal tensile strength	σ_{yt}	430 (MPa)
Transverse tensile strength	$\sigma_{xt} = \sigma_{zt}$	45 (MPa)
Longitudinal compressive strength	σ_{yc}	330 (MPa)
Transverse compressive strength	$\sigma_{xc} = \sigma_{zc}$	80 (MPa)
Shear strength	$\tau_{xy} = \tau_{yz}$	45 (MPa)
	τ_{xz}	60 (MPa)

560 kN · m/rad. Pictures of the joint before and after the static test showed that the pultruded profiles suffered no visible damage (Fig. 10) and that the flexural stiffness of the node was substantially governed by the behavior of the bolted plate because transducers symmetrically placed with respect to the bolted plate recorded small vertical beam displacements comparable to those reported previously for Node A. Strain gauge measurements showed that the upper part of the connection, where there were fewer bolts, was the most stressed area, even if maximum stresses remained below the resistance value of the material. Additionally, the compressive stress distribution due to bolt torques in the direction orthogonal to the plane of elements was representative of the stress distribution on the connection during load application; only the tightening torques of bolts 1, 4, and 6, in the upper part of the joint, were greater than 20 MPa, as shown in Fig. 11.

Comparison of the moment-rotation curves obtained from experimental data on Connections A and B showed that there was a significant difference between the two responses (Fig. 12): the first connection was affected by a consistent loss of initial rotational stiffness due to large stress and strain concentration on the bolted plate, even for small load increments. For this reason, this first connection seemed to be less rigid and less resistant than the second one. Moreover, the damage phenomena on Joint B were very limited and the sudden failure of the bolted plate was accompanied by an important acoustic emission; the damage at the first row of bolts in the upper part confirmed the brittle behavior of the node in the last stage.

Finally, it was observed that the nonlinear behaviors of both connections were very limited: considering the relationship between yielding rotation and plastic rotation (μ) to be a measure of node ductility, as shown in Fig. 12, this ratio was approximately 1.3 in both cases.

Because there was damage to the connection where there were fewer bolts, it was clear that fewer bolts caused a concentration of in-plane stress, leading to local failure of the pultruded elements around the bolt holes, especially where the plate was under tensile stresses. On the plate of Joint A, the damage was more diffused and bearing failure occurred near the edges of both the left and right holes (Fig. 13) for steel bolts equally distributed in the joint zone.

Finite-Element Analysis

Global Model Description

To accurately predict the physical behavior of the bolted joints, a detailed three-dimensional finite-element (FE) model was developed for Connections A and B using *ANSYS 15*. The proposed models were based on the geometry and mechanical properties of elements joined through a bolted plate, and they took into account pretension effect and contact behavior between the FRP and the steel bolts.

The most important geometric details of the structures were modeled by CAD software. The resulting model was then imported into *ANSYS*, where material properties such as mass density, Young's modulus, Poisson's ratio, and shear modulus were assigned to each element. The boundary and loaded conditions for the model were chosen according to the test setup: the lower sides of each bolted plate placed at the beam ends were fixed, and the horizontal displacement increments were applied to the column. Each of these tasks had its own set of issues that affected the ability of the software to converge and give accurate results.

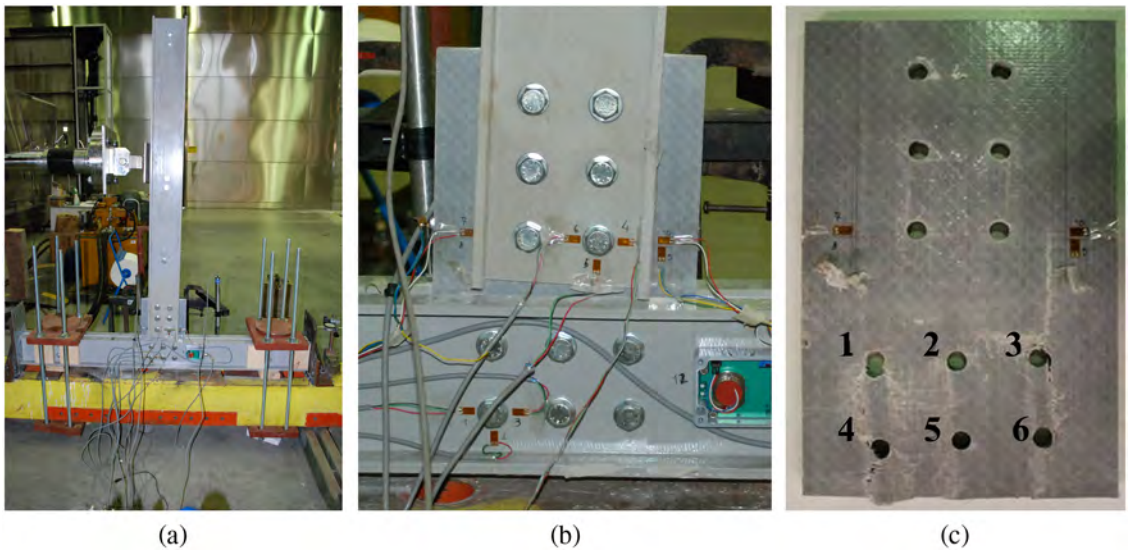

Fig. 6. Failure static test of Connection type A: (a) residual deformation on the node after testing: (b) bolted connection; (c) damage on the bolted plate at the tested end

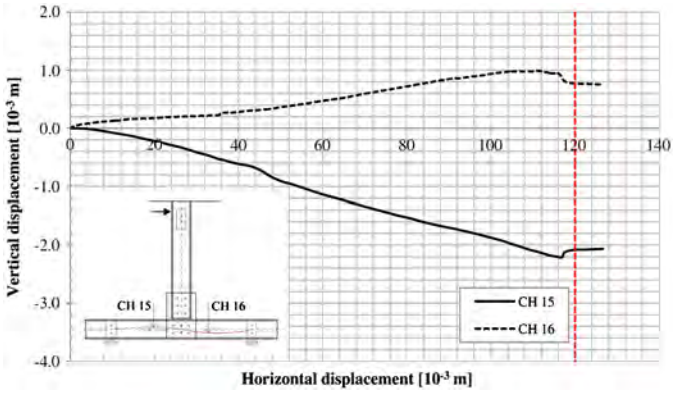

Fig. 7. Measurement of beam deflection by means of two extensometers (CH15 and CH16) symmetrically located with respect to the bolted plate: Connection A

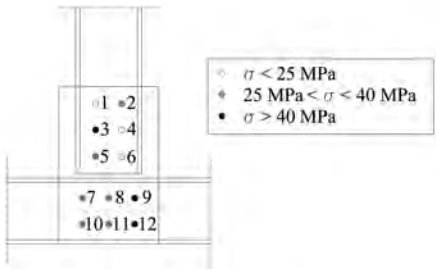

Fig. 8. Perpendicular stress on the surface of the elements due to tightening torques after the failure on Node A

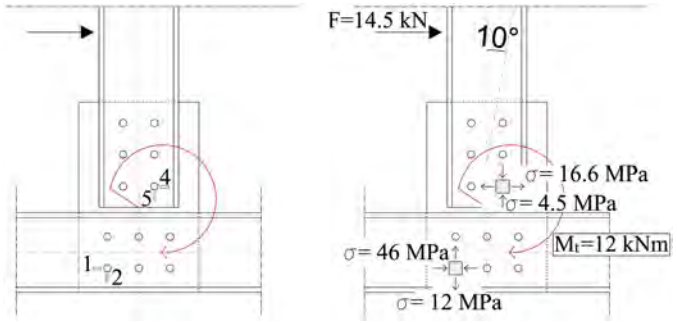

Fig. 9. Maximum state of stress in the profiles derived from the strain gauge placed on Connection A

All three-dimensional components were meshed with tetrahedral solid elements named SOLID187. These elements were defined by 10 nodes having 3 degrees of freedom at each node, with translations in the nodal *x*-, *y*-, and *z*-directions, and were well suited to modeling irregular meshes. Consistent size and shape of the mesh elements on the thread flanks were important for evaluation of load and stress distributions. For this reason, the mesh close to the bolt holes was well refined whereas a less dense mesh was required far from the bolted plate, where the damage phenomena were expected to be less significant. The details are shown in Fig. 14.

Local Model Description

In the three-dimensional model just described, the most significant contacts were those between the FRP flanges and the head, stud, and nut of the bolt. Each steel bolt was made up of a head, stud, and nut; the studs were partially threaded. Because the bearing surface was only between the bolt shank and the pultruded flange, the thread length was not considered in the model (Fig. 15).

In detail, the contact pairs were under-head, stud-to-gusset plate, stud-to-composite, composite-to-gusset plate, under-nut, and stud-to-nut contact regions, as shown in Fig. 15. Because these elements were expected to slide over each other, frictional sliding and asymmetric contact pairs were considered (because steel elements were *target* surfaces). A friction coefficient (k) of 0.2 was assigned to the sliding surfaces (Turvey and Wang 2008).

The surfaces where the profiles were assembled with the plates were highly tightened to prevent surfaces from sliding over each other, so they were considered to be glued together; bolts were not taken into account.

Before applying the incremental load, torque had to be applied to the bolts to avoid initial damage to the cleats due to the crushing of the material in the direction perpendicular to the fibers (the direction in which the strength was lower).

The relationship between applied thread torque and the bolt's preload could be written in terms of bolt diameter and friction coefficient k, so the thread torque of 20 N · m gave a low preload in each bolt. Considering the cross-sectional area of each bolt shank, the preload corresponded to a prestress value of 46 MPa. Pretension could generally be modeled with temperature, constraint equations, or initial strains. In *ANSYS*, the pretension element uses constraint equations and the user creates the element and applies the pretension load. In this approach, an initial displacement is applied to the element. Once the solution starts, the initial displacement is considered part of the load on the model.

Progressive failure analysis uses a failure criterion to predict when the material failure initiates and then reduces the stiffness of the failed material to simulate failure progress through the structure. Different failure criteria have been used in the literature for determining the failure of composite elements (Tsai 1987). The most famous criteria are maximum stress (Agarwal et al. 2006) and maximum strain because they are simple to apply and, more significantly, they describe the mode of failure. However, they neglect the effect of stress interactions. For this reason, these criteria are quite conservative. The interactive criteria, such as Tsai-Wu, Tsai-Hill, and Hoffmann, include stress interactions in the failure mechanism and predict first-ply failure; however, some effort is required to determine the correct input parameters. Among the numerous failure criteria for composite materials in this study, maximum stress was used, according to which failure occurs when at least one stress component along one of the principle material axes reaches the magnitude of corresponding strength in that direction. The stress limit values are given in Tables 1–3.

In *ANSYS* damage evolution is assumed to be an instant stiffness reduction on the basis of the reduction factor for tensile and compressive stiffness in both tension and compression. This value can range from 0 (no damage) to 1 (complete damage). The results refer to a stiffness reduction factor of 0.9. To choose the most suitable value of this factor, some simulations were performed considering stiffness reduction factor values ranging from 0.9 to 0.999. It seemed that 0.9 was the most appropriate value to describe the global behavior of the node because it allowed the analysis to progress even when the damage to the elements was widely diffused.

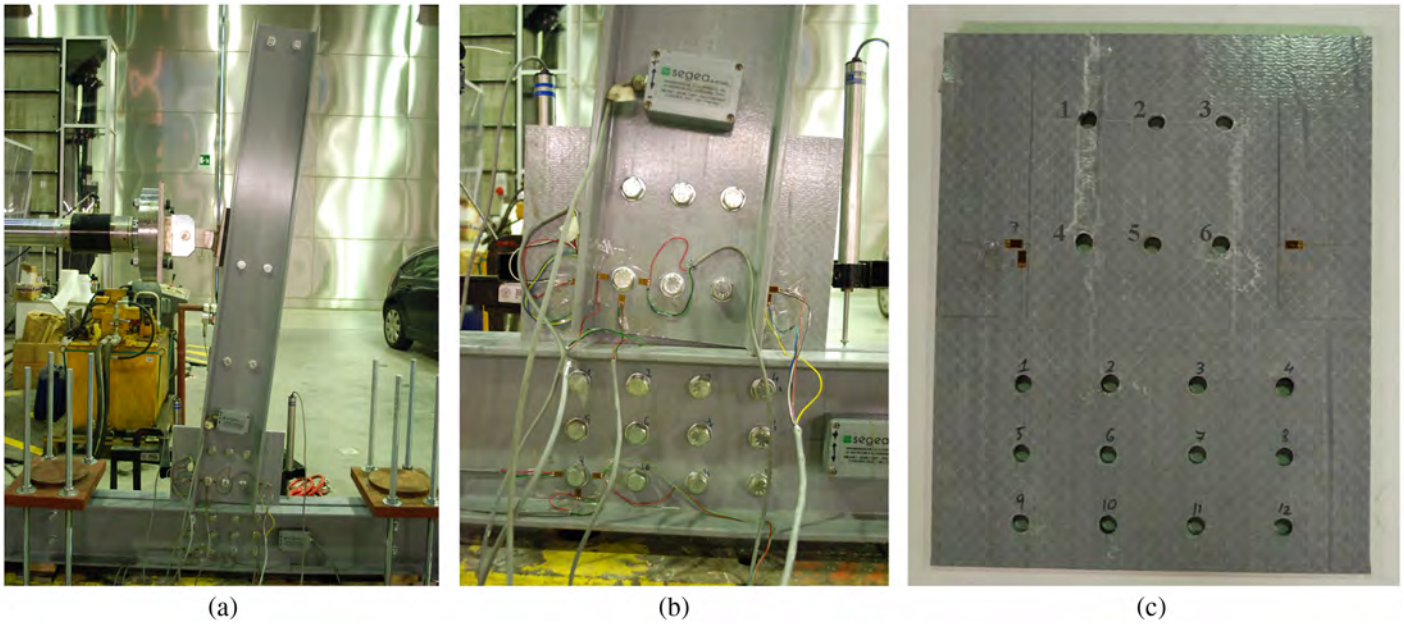

Fig. 10. Static testing of Connection B: (a) residual deformation on the node during testing; (b) bolted connection; (c) damage to the bolted plate at the tested end

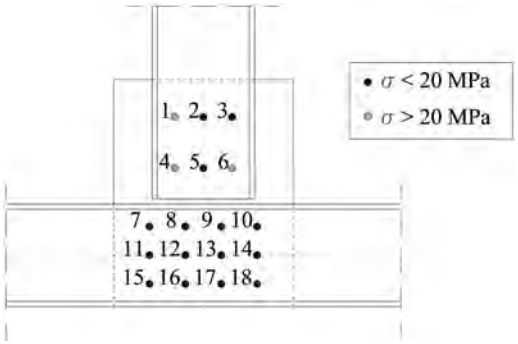

Fig. 11. Perpendicular stress on the surface of the elements due to tightening torques after the failure on Node B

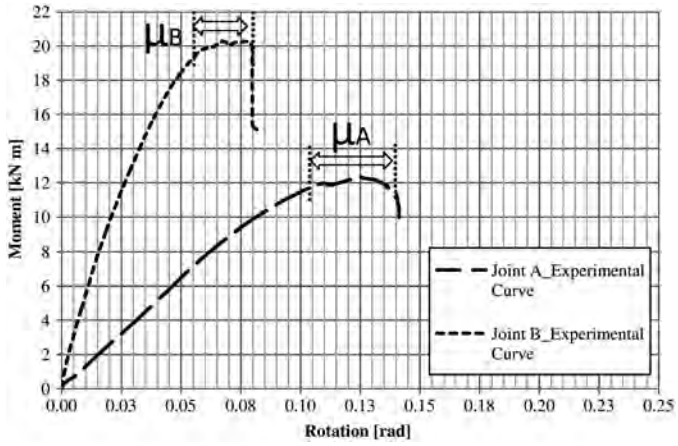

Fig. 12. Comparison of moment-rotation curves obtained from experimental tests on Connections A and B

Finite-Element Model: Comparison of Experimental Results

A comparison of experimental tests and numerical simulations showed that the finite-element model could be used to predict the moment-rotation response of the bolted joints. Furthermore, it was observed that the model was able to enhance prediction of global failure and simulate damage initiation and propagation until complete fracture in the static regime occurred. The good correlation between numerical and experimental results allowed validation of the numerical model, which could even be used to monitor damage propagation in all elements.

For Joint A, Fig. 16 shows that the moment-rotation curve predicted by the numerical model matched quite well the experimental curve in the preliminary test; as for the experimental curve until failure, the moment-rotation curve agreed with the numerical results for the maximum moment (approximately 12 kN · m), whereas it was different from the finite-element model prediction for initial stiffness and ultimate rotation. This result was closely related to the stiffness reduction due to progressive damage to the bolted plate characterized by crushing of the material in the vicinity of the bolt-to-hole interface in the preliminary tests. Based on these observations, it could be assumed that if the node had been subjected to the failure static test directly, without the preliminary tests, the numerical result would have matched the real behavior of the connection.

As for Joint B, excellent agreement was obtained between the numerical moment-rotation response and the experimental data. In both cases, the ultimate moment was 21 kN · m and the initial stiffness was approximately 560 kN · m/rad (Fig. 17).

The finite-element analysis gave a numerical estimate of the node's global behavior, but it could also be used to monitor damage propagation step by step. The failure level could be obtained from the result output according to a legend from 0 (black) when there was no damage to 1 (light gray) if the damage was imminent; white identified areas where failure had already occurred.

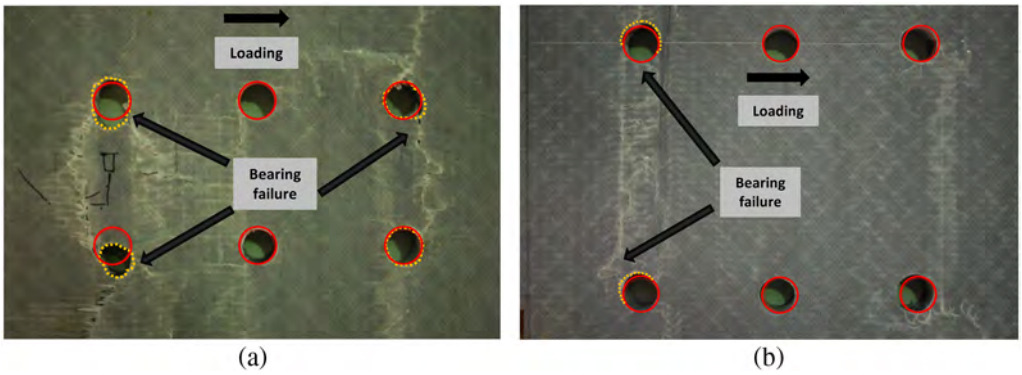

Fig. 13. Comparison of (a) lower part of Plate A and (b) upper part of Plate B where damage occurs, respectively

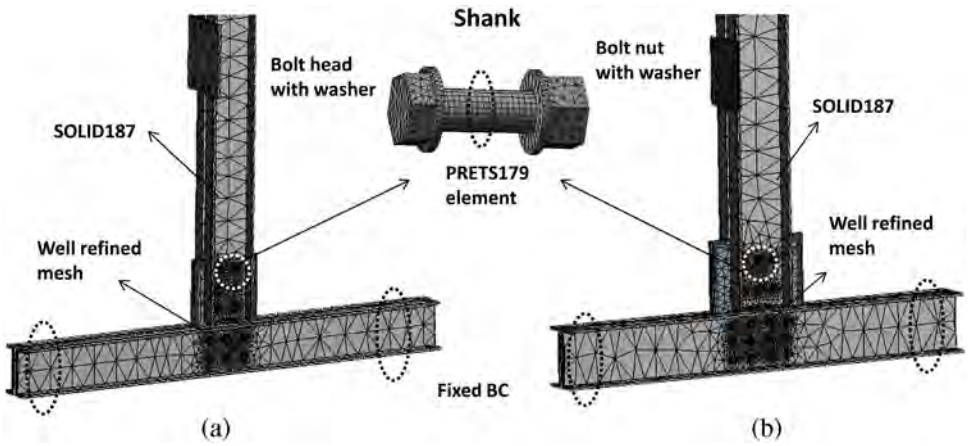

Fig. 14. FEM model of (a) Joint A and (b) Joint B

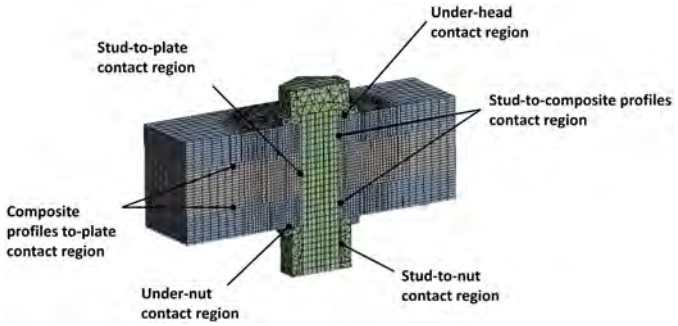

Fig. 15. Solid bolt mesh and cross section of the threaded joint model showing contact regions

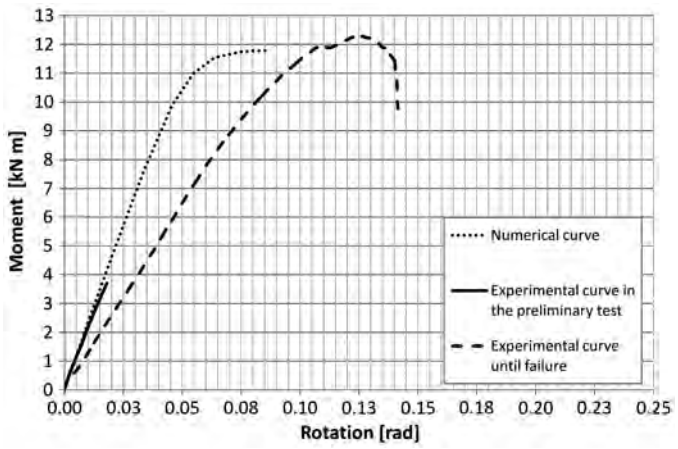

Fig. 16. Comparison of numerical and experimental moment-rotation responses in the preliminary test and the experimental curve until failure for Joint A

When the ultimate moment of Joint A was reached, with regard to the bolted plate, the numerical simulation of damage propagation agreed with the experimental data, as can be seen in Fig. 18. In the upper part of the plate, cracks localized around the head bolt holes; in the lower part, the damage was more extensive, involving bolt rows 7–10 and 9–12. It was clear that the friction between the bolt shank and the hole was the principal factor in damage propagation in the pultruded material.

Fig. 19 compares numerical and experimental results in damage propagation on Joint B. It shows that Bolts 1 and 4 crushed fibers and that a shear-out failure mode occurred in the upper part of the plate. The proposed numerical results predicted the failure mechanism to be fully in agreement with the experimental evidence; the damage concentrated in the upper part of the plate, where the number of bolts was less than in the lower part. The shear-out failure

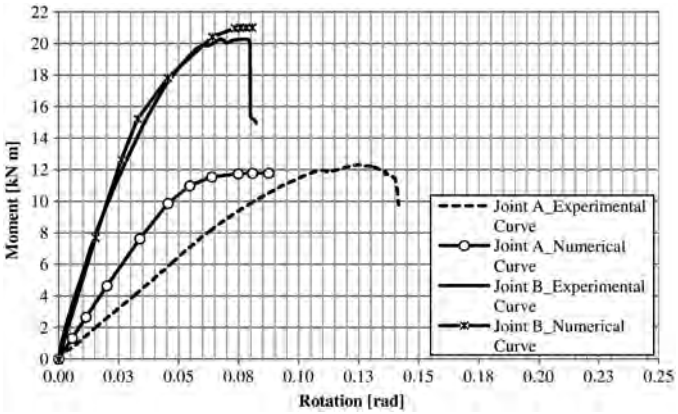

Fig. 17. Comparison of numerical and experimental moment-rotation responses for Joints A and B

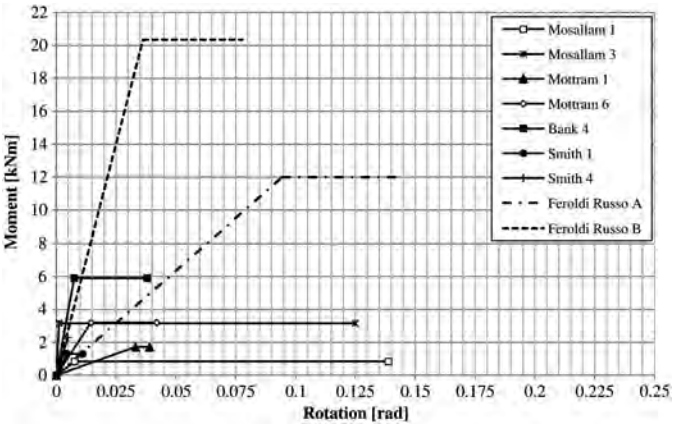

Fig. 20. Comparison of bilinear moment-rotation curves obtained from experimental tests and some curves reported in the literature

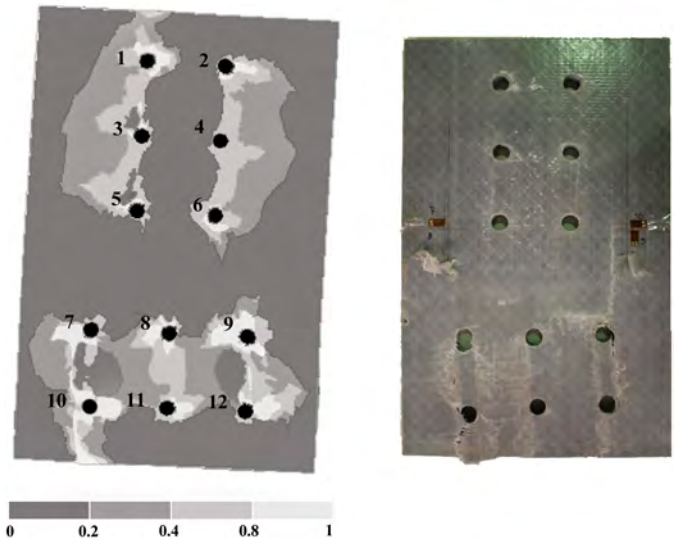

Fig. 18. Comparison of (a) numerical and (b) experimental results for damage propagation on the bolted plate (Joint A)

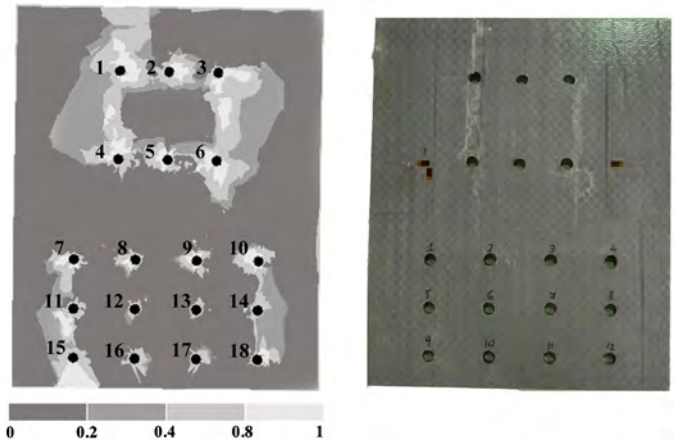

Fig. 19. Comparison of (a) numerical and (b) experimental results for damage propagation on the bolted plate (Joint B)

mode involved only the bolted plate in the area where fewer bolts determined a stress localization, and thus failure occurred as a consequence of localized damage.

Discussion

The two joint configurations, although characterized by different moment-rotation laws, were both significantly influenced by the behavior of the pultruded plate. As a consequence, the moment-rotation law was not affected by the flexural deformation of the column or by the deformation of the beam to which it was connected.

In Joint A, widespread damage was observed, especially in the lower part of the connection plate, where the bending moment was maximum. This was expected because the part farthest from the point of force application was the most stressed of the connection. Joint B exhibited instead a local shear-out failure mode in the upper part of the bolted plate, where the column and beam were connected by means of 6 steel bolts; the asymmetric arrangement of steel bolts between the portion of the plate connected to the column and the portion connected to the beam ensured that the damage concentrated where there were fewer bolts. It was clear that a symmetric bolt arrangement was better than an asymmetric arrangement because it induced a uniform stress distribution, leading to a less brittle failure mechanism.

The influence of fiber orientation on the failure mode was crucial; when the orientation was in the pultruded direction along the height of the plate, the bolts crushed the composite material. This was a typical failure mode of bolted joints with composite plates (i.e., the bearing mode). In detail, local bearing failure mode was characterized by crushing of the material in the vicinity of the bolt-to-hole interface; in other words, a shear-out failure occurred characterized by the shear-out part of the composite ahead of the bolt.

Regardless of the failure modes that influence the nonlinearity of the moment-rotation law, it was interesting to compare the curves obtained with those reported in the literature (Turvey and Cooper 2004). The beam-to-column bolted joints shown in Fig. 20 were between the GRP beams and columns, and the flange cleats either were cut from the pultruded angle section or used universal columns elements. All of these joints had a similar layout but differed with respect to material, number, and diameter of bolts (pultruded or steel), as well type of connection (only bolted or bolted

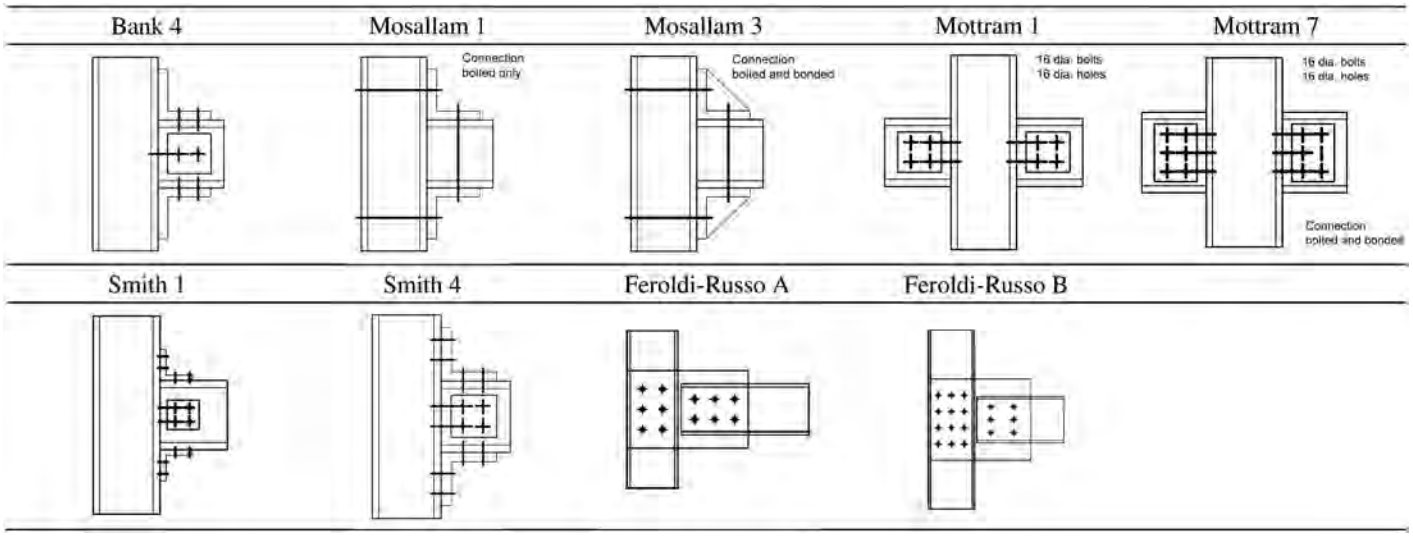

Fig. 21. Beam-to-column joint layouts discussed and compared with those analyzed in this paper

and adhesively bonded). For example, in Mosallam 1 and 3 and in Bank 4, the bolted joints were between GRP WF-section beams and columns connected by pultruded GRP threaded rods, whereas Mottram used steel bolts and WF-section profiles; in Smith the steel bolted web and flange cleat joints were between pultruded GRP I-section beams and columns (Fig. 21). These configurations were compared to joints tested in the present work; the comparison showed that the respective stiffness of Joints A and B was in the same range as in other test configurations, but the joints' flexural strength could be up to 20 times higher.

Conclusions

In this paper, an experimental and numerical study of the behavior of two different beam-column bolted joints through an FRP pultruded plate was presented. Based on the results of the analysis, the conclusions described in the following paragraphs can be proposed.

Experimental and numerical results showed that in both joints the global behavior of the connection was substantially influenced by damage progression in the FRP pultruded plate. At initial loading steps, there was little friction resistance and slipping of the connections occurred. Both connections behaved linearly because they failed when the bolts crushed the composite material, which failed in shear-out mode.

Instruments used during the experimental tests confirmed that the global behavior of the joints was not influenced by the stiffness of pultruded profiles; deformations associated with flexure were not observed over all displacements applied to the joints, nor did instability in compressed members appear. This result was desired to emphasize the performance of the bolted FRP pultruded plate, which first influenced the connection as a whole.

As expected, a symmetric bolt arrangement in the FRP pultruded plate induced the highest stress concentrations and failure propagation in the lower part of the plate, where the moment was maximum.

An asymmetric bolt arrangement induced a different failure mechanism—because damage concentrated where there were fewer bolts—in the upper portion of the plate connected to the column. Because stresses and cracks concentrated at few points, the final failure of the joint was sudden and characteristically brittle, with a non-negligible acoustic emission.

The M-θ response of each connection was predicted using an FE model, which accounted for the pretension effect and frictional contacts between the composite and steel surfaces. A good match between experimental and numerical results was observed on both structural profiles and the bolted plate; thus, the chosen failure criterion could be considered satisfactory.

For bolted connections between pultruded profiles, the use of an FRP pultruded plate placed between the webs of the elements, instead of between the web and the flange cleats, is certainly a novelty and leads to the discovery of new mechanisms of failure. Both the experimental and numerical results of this study show that the global behavior of beam-to-column joints is substantially influenced by damage progression in the FRP pultruded plate whereas the column rigidly rotates and the beam remains in its original configuration.

On the basis of the type of joint collapse and the local damage in each FRP pultruded plate, the use of a gusset plate instead of a pultruded one presumably can be related to a general improvement in the performance of this type of complex connection.

Acknowledgments

The authors would like to express their gratitude and sincere appreciation to TopGlass (Top Glass S.p.A., Osnago, Italy) for providing the material used in the experimental tests. Special thanks go to the staff of LabSCo for their crucial help and special suggestions regarding this research work.

References

Adilardi, A., and Russo, S. (2010). "Innovative design approach to a GFRP pedestrian bridge: Structural aspects, engineering optimization and maintenance." *Proc., 15th Int. Conf. on Bridge Maintenance, Safety and Management*, CRC Press/Balkema, Taylor and Francis Group, Leiden, Netherlands, 2455–2459.

Agarwal, B. D., Broutman, L. J., and Chandrashekhara, K. (2006). *Analysis and performance of fiber composites*, Wiley, New York.

ANSYS 15 [Computer software]. Canonsburg, PA, ANSYS.

ASCE. (1984). "Structural plastic design manual." Reston, VA, 1176.

Bank, L. C. (2006). *Composites for construction-structural design with FRP materials*, Wiley, Hoboken, NJ.

Boscato, G., Mottram, J. T., and Russo, S. (2011). "Dynamic response of a sheet pile of fiber-reinforced polymer for waterfront barriers." *J. Compos. Constr.*, 10.1061/(ASCE)CC.1943-5614.0000231, 974–984.
Boscato, G., and Russo, S. (2008). "On mechanical performance of different type of FRP beams as reinforcement of pedestrian bridge." *Proc., 14th Int. Conf. on Bridge Maintenance, Safety and Management*, Bridge Maintenance, Safety Management, Health Monitoring and Informatics, Seoul.
Boscato, G., and Russo, S. (2009). "Free vibrations of pultruded FRP elements: Mechanical characterization, analysis, and applications." *J. Compos. Constr.*, 10.1061/(ASCE)1090-0268(2009)13:6(565), 565–574.
Boscato, G., and Russo, S. (2013). "Free vibrations of a pultruded GFRP frame with different rotational stiffnesses of bolted joints." *Mech. Compos. Mater.*, 48(6), 655–668.
Boscato, G., Russo, S., and Mottram, J. T. (2012). "Design and free vibration of a large temporary roof FRP structure for the Santa Maria Paganica church in L'Aquila." *Proc., 6th Int. Conf. on FRP Composites in Civil Engineering (CICE 2012)*, IIFC (International Instute for FRP in Construction), Kingston, ON, Canada, 8.
Cooper, C., and Turvey, G. J. (1995). "Effects of joint geometry and bolt torque on the structural performance of single bolt tension joints in pultruded GRP sheet material." *Compos. Struct.*, 32(1), 217–226.
Dicuonzo, A., Laudiero, F., Minghini, F., and Tullini, N. (2008). "Design and construction of a temporary structure composed by FRP pultruded profiles." *Proc., 4th Int. Conf. on FRP Composites in Civil Engineering (CICE 08)*, EMPA, Zurich, Switzerland.
Di Tommaso, A., and Russo, S. (2003). "Shape influence in buckling of GFRP pultrudes columns." *Mech. Compos. Mater.*, 39(4), 329–340.
Keller, T. (2003). "Use of fibre reinforced polymers in bridge construction." International Association for Bridge and Structural Engineering (IABSE-AIPC-IVBH), Zurich, Switzerland.
Khashaba, U. A., Sallam, H. E. M., Al-Shorbagy, A. E., and Seif, M. A. (2006). "Effect of washer size and tightening torque on the performance of bolted joints in composite structures." *Compos. Struct.*, 73(3), 310–317.
Mottram, J. T., and Zheng, Y. (1996). "State-of-the-art review on the design of beam-to-column connections for pultruded frames." *Compos. Struct.*, 35(4), 387–401.
Qureshi, J., and Mottram, J. T. (2013). "Behaviour of pultruded beam-to-column joints using steel web cleats." *Thin-Walled Struct.*, 73(12), 48–56.
Qureshi, J., and Mottram, J. T. (2014). "Response of beam-to-column web cleated joints for FRP pultruded members." *J. Compos. Constr.*, 10.1061/(ASCE)CC.1943-5614.0000392, 04013039.
Qureshi, J., and Mottram, J. T. (2015). "Moment-rotation response of nominally pinned beam-to-column joints for frames of pultruded fibre reinforced polymer." *Constr. Build. Mater.*, 77(2), 396–403.
Russo, S. (2011). "Performance of a PFRP structure covering a historic building struck by an earthquake." *Proc., 5th Int. Conf. Advanced Composites in Construction*, NetComposites, Chesterfield, U.K., 51–57.
Russo, S. (2012). "Experimental and finite element analysis of a very large pultruded FRP structure subjected to free vibration." *Compos. Struct.*, 94(3), 1097–1105.
Russo, S. (2013). "Damage assessment of GFRP pultruded structural elements." *Compos. Struct.*, 96, 661–669.
Tsai, S. W. (1987). *Composites design*, 3rd Ed., Think Composites, Dayton, OH.
Turvey, G. J., and Cooper, C. (2004). "Review of tests on bolted joints between pultruded GRP profiles." *Proc. Inst. Civ. Eng.: Struct. Build.*, 157(3), 211–233.
Turvey, G. J., and Wang, P. (2008). "An FE analysis of the stresses in pultruded GRP single-bolt tension joints and their implications for joint design." *Comput. Struct.*, 86(9), 1014–1021.